

A Regional Ocean–Atmosphere Model for Eastern Pacific Climate: Toward Reducing Tropical Biases*

SHANG-PING XIE,^{+,#} TORU MIYAMA,[@] YUQING WANG,^{+,#} HAIMING XU,^{&,+} SIMON P. DE SZOEKE,⁺
R. JUSTIN O. SMALL,⁺ KELVIN J. RICHARDS,^{+,**} TAKASHI MOCHIZUKI,[@] AND TOSHIYUKI AWAJI^{@,++}

⁺ International Pacific Research Center, University of Hawaii at Manoa, Honolulu, Hawaii

[#] Department of Meteorology, University of Hawaii at Manoa, Honolulu, Hawaii

[@] Frontier Research Center for Global Change, Yokohama, Japan

[&] Department of Atmospheric Sciences, Nanjing University of Information Science and Technology, Nanjing, China

^{**} Department of Oceanography, University of Hawaii at Manoa, Honolulu, Hawaii

⁺⁺ Department of Geophysics, Kyoto University, Kyoto, Japan

(Manuscript received 24 March 2006, in final form 13 September 2006)

ABSTRACT

The tropical Pacific Ocean is a climatically important region, home to El Niño and the Southern Oscillation. The simulation of its climate remains a challenge for global coupled ocean–atmosphere models, which suffer large biases especially in reproducing the observed meridional asymmetry across the equator in sea surface temperature (SST) and rainfall. A basin ocean general circulation model is coupled with a full-physics regional atmospheric model to study eastern Pacific climate processes. The regional ocean–atmosphere model (ROAM) reproduces salient features of eastern Pacific climate, including a northward-displaced intertropical convergence zone (ITCZ) collocated with a zonal band of high SST, a low-cloud deck in the southeastern tropical Pacific, the equatorial cold tongue, and its annual cycle. The simulated low-cloud deck experiences significant seasonal variations in vertical structure and cloudiness; cloud becomes decoupled and separated from the surface mixed layer by a stable layer in March when the ocean warms up, leading to a reduction in cloudiness. The interaction of low cloud and SST is an important internal feedback for the climatic asymmetry between the Northern and Southern Hemispheres. In an experiment where the cloud radiative effect is turned off, this climatic asymmetry weakens substantially, with the ITCZ migrating back and forth across the equator following the sun. In another experiment where tropical North Atlantic SST is lowered by 2°C—say, in response to a slow-down of the Atlantic thermohaline circulation as during the Younger Dryas—the equatorial Pacific SST decreases by up to 3°C in January–April but changes much less in other seasons, resulting in a weakened equatorial annual cycle. The relatively high resolution (0.5°) of the ROAM enables it to capture mesoscale features, such as tropical instability waves, Central American gap winds, and a thermocline dome off Costa Rica. The implications for tropical biases and paleoclimate research are discussed.

1. Introduction

The climatology of the Pacific is characterized by large zonal and meridional asymmetries, with an eastern equatorial cold tongue and a northern intertropical convergence zone (ITCZ). Ocean–atmosphere interac-

tion plays an important role in generating and maintaining these asymmetric features despite a solar radiation forcing at the top of the atmosphere that is zonally uniform and nearly symmetrical about the equator in the annual mean. Along the equator, the interaction of the eastern cold tongue and easterly winds is key to maintaining the zonal asymmetry (Dijkstra and Neelin 1995; Sun and Liu 1996), much as it is in developing ENSO (Neelin et al. 1998; Wang and Picaut 2004). Ocean dynamics, the equatorial upwelling, and the eastward shoaling thermocline in particular are important for this Bjerknes feedback. The northward-displaced ITCZ, on the other hand, is associated with a meridional asymmetry in sea surface temperature

* IPRC/SOEST Contribution Numbers 413/6918.

Corresponding author address: Shang-Ping Xie, International Pacific Research Center, SOEST, University of Hawaii at Manoa, Honolulu, HI 96822.
E-mail: xie@hawaii.edu

(SST), with warm water on the north and much colder water on the south side of the equator. The interaction of ocean mixed-layer temperature and surface heat flux is important for maintaining this north–south asymmetry (Xie and Philander 1994; Philander et al. 1996). The northward-displaced ITCZ maintains southerly cross-equatorial winds, whose strength varies in response to seasonal variations in insolation, resulting in a pronounced annual cycle in SST (Mitchell and Wallace 1992; Xie 1994). The warm and cold phases of this annual cycle are March and September, respectively. During a brief period from March to April, the eastern tropical Pacific climate becomes rather symmetrical, with an ITCZ forming over a warm SST band on either side of the equator. Mitchell and Wallace (1992) describe the basic features of eastern tropical Pacific climate while Xie (2004) reviews the underlying coupled dynamics.

Despite the climatic importance of the eastern Pacific, its simulation in state-of-the-art coupled ocean–atmosphere general circulation models (GCMs) remains unsatisfactory. Instead of staying in the Northern Hemisphere during most of the year, model ITCZs tend to move across the equator following the seasonal march of the sun and the southern ITCZ persists too long compared to observations, resulting in a double ITCZ in the annual mean and attendant warm biases in SST over the southeast Pacific off South America (Mechoso et al. 1995; W. Wang et al. 2005; Wittenberg et al. 2006; Large and Danabasoglu 2006). This double ITCZ syndrome persists in a recent assessment of coupled models participating in the Intergovernmental Panel on Climate Change (IPCC) Fourth Assessment Report (AR4; S. P. de Szoeke, personal communication). In some models, this reduced latitudinal asymmetry is associated with the westward displacement of the equatorial cold tongue and an erroneous semiannual cycle in this cold tongue. These tropical biases limit the skill of ENSO simulations by these models as the mean state and seasonal cycle of the equatorial Pacific are known to affect properties of ENSO, such as its period, amplitude, and seasonality (Jin et al. 1994; Chang et al. 1994; Li and Hogan 1999; Timmermann et al. 2006, manuscript submitted to *J. Climate*). For example, interannual variance of equatorial SST in some coupled GCMs peaks in seasons other than November–January (Saji et al. 2006), altering the ENSO's teleconnection into the extratropics.

Sources of these tropical biases include the poor representation of land orography and ocean–atmospheric processes and their interaction in the GCMs. Atmospheric models that use a terrain-following sigma coordinate with typical horizontal resolutions of 2°–3° suffer

large numerical errors near narrow and steep mountains. Using a moderately high resolution (0.5°) model, Xu et al. (2004) show that the steep Andes help maintain the South Pacific stratus cloud deck in August–October (Richter and Mechoso 2006), an effect in favor of a northward-displaced ITCZ. The alongshore wind on the west coast of South America is a major mechanism that keeps the tropical Pacific cool south of the equator, but it is subject to large numerical errors because of the Andes to its east (Large and Danabasoglu 2006). The South Pacific stratus cloud deck and equatorial upwelling are among the physical processes that GCMs have difficulty simulating. Studies show that the reduction in solar radiation under the South Pacific stratus cloud deck is key to keeping the ITCZ north of the equator in coupled GCMs (Philander et al. 1996; Ma et al. 1996; Yu and Mechoso 1999; Gordon et al. 2000).

The present paper describes a regional ocean–atmosphere model (ROAM) developed at the University of Hawaii's International Pacific Research Center (IPRC) and demonstrates with examples its utility in studying air–sea processes in the eastern tropical Pacific. The regional model domain affords the use of 0.5° resolution for both the atmosphere and ocean components. This is equivalent to triangle truncation at zonal wavenumber 215 (T215) for global spectral models, 5 times higher than most of atmospheric GCMs in use. This resolution is still marginal to resolve narrow mountain ranges of Central and South Americas but allows us to begin exploring their effects on the coupled system. A relatively high resolution also enables us to study mesoscale features in the ocean and atmosphere, such as the equatorial SST front and its meanders, Central American gap winds, and the Costa Rica Dome in the ocean thermocline.

The model is restored toward observations on open boundaries. One might question whether this restoring would guarantee a realistic simulation. We suggest for the following reasons, and our results support, that the lateral restoring is not strong enough to dictate the latitudinal asymmetry and the equatorial annual cycle of the model, and that the ROAM is an adequate tool for studying these features. First, the regional atmospheric model has a fairly large domain of 70° latitude \times 120° longitude so the ROAM has enough freedom to develop its own climatology. Second, previous studies show that to first order, latitudinal asymmetry and the equatorial annual cycle originate from air–sea–land interaction in the eastern Pacific. Xie (1996) proposes a westward control theory for the development of latitudinal asymmetry based on the fact that large-scale antisymmetrical perturbations propagate only westward

as Rossby waves. Indeed, coupled model results confirm that such westward-traveling coupled waves displace the ITCZ north of the equator and establish the basinwide latitudinal asymmetry (Ma et al. 1996; Kimoto and Shen 1997; Xie and Saito 2001). The equatorial annual cycle in SST is basically a coupled response to solar-induced variations in cross-equatorial wind, with large amplitudes in the east and a characteristic westward propagation (Mitchell and Wallace 1992; Xie 1994). Our experiments show that the removal of key air–sea feedback processes causes the model climate to deviate substantially from observations, indicating that the lateral boundary forcing does not dictate model simulations.

This paper describes the model construction, evaluates its performance against observations, and highlights some of the model applications. More detailed and thorough analyses will be presented elsewhere. The rest of the paper is organized as follows. Section 2 introduces the ocean and atmospheric models and describes their coupling. Section 3 presents the model climatology and compares it with observations. Section 4 investigates the model sensitivity to internal feedbacks and external forcing, while Section 5 illustrates the model's utility to study mesoscale phenomena. Sections 3–5 are written to be self contained and interested readers may skip to section(s) most interesting to them. Section 6 is a summary.

2. Regional coupled model

The IPRC ROAM (iROAM) couples a regional atmospheric model with a Pacific basin ocean GCM. This section briefly introduces the atmospheric and ocean components and then describes their coupling.

a. Atmospheric regional model

We use the IPRC regional atmospheric model (iRAM; formerly called the IPRC regional climate model). The iRAM solves hydrostatic primitive equations in spherical coordinates in the horizontal and in a terrain-following sigma (pressure divided by surface pressure) coordinate in the vertical. It uses an unstaggered $0.5^\circ \times 0.5^\circ$ grid and has 28 vertical levels with 11 of them below 800 hPa to represent the atmospheric boundary layer (ABL) and low clouds. The model domain covers one-third of the global tropical belt, extending from 35°S to 35°N , 150° to 30°W . The U.S. Geological Survey high-resolution topographic dataset on a $1/12^\circ$ grid is used to construct envelope topography by adding standard deviation to the grid-mean topography. The grid-mean topography tends to underestimate orographic effects.

The model physics include the cloud microphysics

scheme of Wang (2001); a mass flux parameterization scheme for subgrid shallow, midlevel, and deep convection developed by Tiedtke (1989) and modified by Nordeng (1995) for a CAPE closure for deep convection; the radiation package developed by Edwards and Slingo (1996) and improved by Sun and Rikus (1999); the Biosphere–Atmosphere Transfer Scheme (BATS) of Dickinson et al. (1993) for land surface processes; a modified Monin–Obukhov similarity scheme (Fairall et al. 2003) for surface flux calculations over the ocean; and a nonlocal $E-\epsilon$ turbulence closure scheme for subgrid vertical mixing (Langland and Liou 1996). Cloud amount is diagnosed using the Xu and Randall (1996) semiempirical parameterization scheme. To improve the ABL cloud simulation, modifications were made to the shallow convection parameterization as documented in Wang et al. (2004a,b).

Wang et al. (2004b) investigate the sensitivity of ABL cloud simulation to changes in horizontal and vertical resolution, parameterizations of ABL turbulence, shallow convection, and cloud microphysics. The vertical structure and cloudiness of ABL clouds are found to be sensitive to the treatment of shallow convection and drizzle. Clouds are too thin over the ocean near the west coast of South America in the iRAM. The auto-conversion of cloud water to rain depends on cloud droplet number concentration following Tripoli and Cotton's (1980) parameterization. The cloud droplet number concentration is gradually increased in a 1000-km-wide coastal zone from the open ocean value of 10^{-8} m^{-3} to $3 \times 10^{-8} \text{ m}^{-3}$ on the coast to mimic the dispersion of aerosols of continental origin. These numbers are comparable to estimates based on satellite observations (Miles et al. 2000). This change leads to a thickening of ABL cloud in a narrow coastal zone (section 3b) but turns out to have little effect on cloud farther offshore. Nor does it affect the overall performance of the coupled model.

We refer to Wang et al. (2004a,b) for a detailed description of the iRAM. It has been tested over the eastern tropical Pacific and used to study the atmospheric adjustment to the equatorial front north of the equator (Small et al. 2005) and its meanders due to tropical instability waves (Small et al. 2003), ABL clouds over the southeast Pacific (Wang et al. 2004a,b), and orographic effects of the Andes (Xu et al. 2004) and Central American mountains (Xu et al. 2005). In these studies the iRAM simulations compare quite well with available in situ/satellite observations.

b. Ocean model

The version 2 of the Geophysical Fluid Dynamics Laboratory Modular Ocean Model (MOM2; Pac-

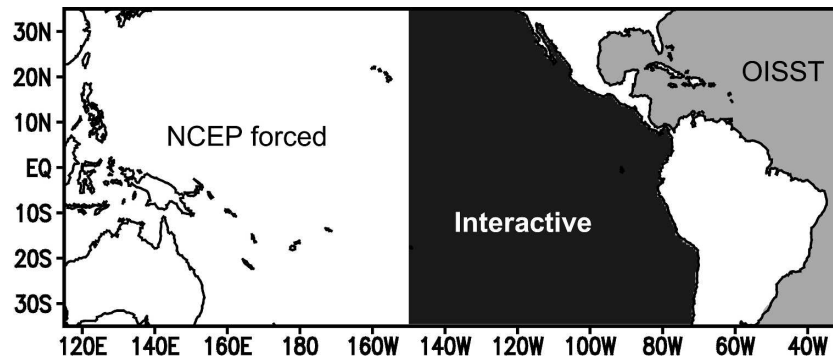


FIG. 1. Model configuration. The ocean and atmospheric components are fully interactive in the eastern Pacific east of 150°W . The ocean model is forced with the NCEP–NCAR reanalysis in the western basin while the atmospheric model is forced by the OISST in the Atlantic.

anowski 1996) is used. The horizontal grid spacing is 0.5° longitude by 0.5° latitude. There are 30 levels in the vertical, with 20 of them in the upper 400 m. Harmonic lateral mixing is used with constant viscosity and diffusivity of $2 \times 10^6 \text{ cm}^2 \text{ s}^{-1}$. Vertical mixing is based on the Pacanowski and Philander (1981) parameterization. The background viscosity and diffusivity are set at 1 and $0.01 \text{ cm}^2 \text{ s}^{-1}$, respectively.

The ocean model domain covers the entire tropical Pacific between 35°N and 35°S . The MOM2 employs the staggered B grid and we let the horizontal grid for temperature, salinity, and their surface fluxes be collocated with the unstaggered atmospheric grid, simplifying the flux exchange between the ocean and atmosphere. Near the northern and southern boundaries, temperature and salinity are restored toward the monthly climatology of Levitus (1982). The restoring factor is reduced linearly from $1/(15 \text{ days})$ on the boundaries to zero 10° equatorward.

The ocean GCM is spun up for 5 yr from 1991 through 1995, from an initial resting state with the January temperature and salinity climatology of Levitus (1982). Surface salinity is restored to the Levitus (1982) monthly climatology with a time constant of 30 days. At the sea surface we use the daily mean wind stress and radiative fluxes derived from the National Centers for Environmental Prediction–National Center for Atmospheric Research (NCEP–NCAR) reanalysis (Kalnay et al. 1996). Surface turbulent heat flux is calculated using the reanalysis wind speed, air temperature, and humidity at 10 m along with the model SST.

c. Coupling

From 1 January 1996 onward, the same NCEP surface variables continue to force the ocean model outside the iRAM domain. East of 150°W , the ocean GCM and iRAM are interactive, exchanging daily mean

fluxes once every day (Fig. 1). Surface salinity is restored toward the Levitus (1982) climatology, a constraint we plan to remove in the future. Weekly SST values based on the Reynolds et al. (2002) dataset are prescribed in the tropical Atlantic (section 4 investigates the model sensitivity to Atlantic SST). On the iRAM's lateral boundaries, atmospheric temperature, humidity, and wind velocity are restored toward the NCEP–NCAR reanalysis in a buffer zone 6° wide, in which the restoring coefficient vanishes exponentially toward the interior. The reference data in the buffer zones are updated 4 times daily.

The regionally coupled model is integrated for 8 yr from 1996 through 2003. Hereafter this integration is referred to as the control run. Figure 2 compares the SST time series averaged in the Niño-3 (5°S – 5°N , 150° – 90°W) region between the iROAM simulation and observations of Reynolds et al. (2002). The iROAM SST is 1° – 2°C too cold for the first 2 yr but shows a good agreement with observations in subsequent years. The simulation of the equatorial annual cycle, in particular, agrees well with observations. The iROAM SST is about 0.5°C too warm in some years compared to observations during the cold phase of the annual cycle and, interestingly, this bias is smaller than in the ocean model spin-up run forced by the reanalysis (from 1991 through 1995).

Despite a cold bias in absolute SST, the model captures the major 1997–98 El Niño event very well, both in amplitude and phase. This is not surprising since the ocean GCM is forced with observed wind and heat flux in the western half of the tropical Pacific, where large wind anomalies associated with ENSO are observed (Wallace et al. 1998). Wind anomalies near the date line force oceanic Kelvin waves that propagate into the eastern Pacific, depress the thermocline, and cause large warming. Thus, the western tropical Pacific,

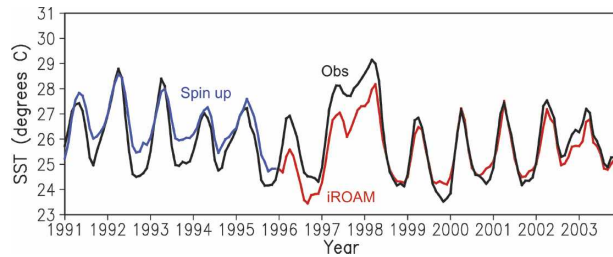


FIG. 2. Niño-3 SST ($^{\circ}\text{C}$) averaged in 5°S – 5°N , 150° – 90°W in the iROAM control run and observations.

though not directly coupled with the iRAM, communicates with the interactive eastern domain via ocean waves. In the climatological mean, the easterly winds in the western basin help the iROAM maintain the eastward shoaling of the thermocline and the cold tongue on the equator. For this reason the Walker circulation and ENSO are not the foci of this paper. Instead we study the latitudinal asymmetry of eastern Pacific climate and the equatorial annual cycle, for which eastern Pacific processes are of first-order importance (Mitchell and Wallace 1992; Xie 2004).

The lateral restoration of the iRAM to observations, the prescribed Atlantic SST, and very importantly, internal air–sea interactions all contribute to the realistic model simulation. The iRAM’s lateral boundary conditions influence air temperature in the free troposphere via wave adjustment, but air temperature and humidity in the ABL are strongly interactive with the ocean in the coupled domain. As will be shown in section 4, ocean–atmospheric feedback within the eastern Pacific is very important in setting the latitudinal asymmetry of SST in the iROAM.

Because of strong air–sea coupling, tropical Pacific climate adjusts rather rapidly to a quasi-steady state in 1 to 2 yr in global coupled GCMs whose components are properly spun up (Ma et al. 1996; Xie and Saito 2001; Large and Danabasoglu 2006). In the iROAM, this spinup time is likely to be shorter because observed winds are used to drive the western half of the ocean basin and the climate over the interactive eastern basin is quite realistic. Thus, we use the 6-yr simulation from 1998 to 2003 to construct the climatology, a period that happens to coincide roughly with the Tropical Rainfall Measuring Mission (TRMM) and Quick Scatterometer (QuikSCAT) satellite observations.

The iROAM’s 0.5° resolution is modest compared to that of the most advanced atmospheric GCMs ($\sim 0.1^{\circ}$), such as the Atmospheric GCM for the Earth Simulator (AFES; Ohfuchi et al. 2004) and the National Aeronautics and Space Administration’s (NASA) finite-volume GCM (fvGCM; Shen et al. 2006), the latter

models being run in the weather forecast mode. It is still better than global coupled GCMs in resolution, most run at T42 but some at T106 (Luo et al. 2005; Sakamoto et al. 2004). Generally, regional and global coupled models offer complementary experimental designs; the former is forced at lateral boundaries and achieves better realism, while the latter is free running but may deviate significantly from observations.

d. Validation data

For comparison with the control run, we use the monthly climatology of the TRMM 3B43 precipitation product from December 1997 to August 2005 and QuikSCAT surface wind velocity from August 1999 to August 2005, both on a 0.25° grid. The 3B43 product uses the TRMM and other microwave sensors to adjust infrared observations by geostationary satellites and combines ground rain-gauge measurements (Kummerow et al. 2000). The QuikSCAT measures the surface wind speed and direction under all weather conditions except under heavy rainfall (Liu et al. 2000; Chelton et al. 2001). We use Reynolds et al.’s (2002) optimum interpolation SST (OISST) analysis on a 1° grid, ship reports of cloudiness in the Comprehensive Ocean–Atmospheric Data Set on a 2° grid (COADS; Woodruff et al. 1987), and surface solar radiation derived from International Satellite Cloud Climatology Project (ISCCP) observations (Zhang et al. 2004).

3. Climatology

Figure 3 compares annual mean SST, precipitation, and surface wind velocity between the iROAM’s control run and observations. The model captures the salient features of eastern Pacific climate including the equatorial cold tongue and the northward-displaced rainband. The hydrological cycle in the model is too strong, with precipitation in the ITCZ about 40% above the observations (note different color scales in Figs. 3a,b). This bias in rainfall is present when the atmospheric model is forced by prescribed SST and associated with a bias in surface wind speed that is about 1 m s^{-1} too strong compared to QuikSCAT (Small et al. 2003).

The simulated eastern Pacific climate is highly asymmetric about the equator. There is a zonal band of warm water with SST greater than 27°C around 10°N that supports deep convection in the ITCZ. On the other side of the equator, by contrast, SST is significantly lower and precipitation substantially weaker. The greatest SST contrast is found between the Central and South American coasts: the northern high-SST

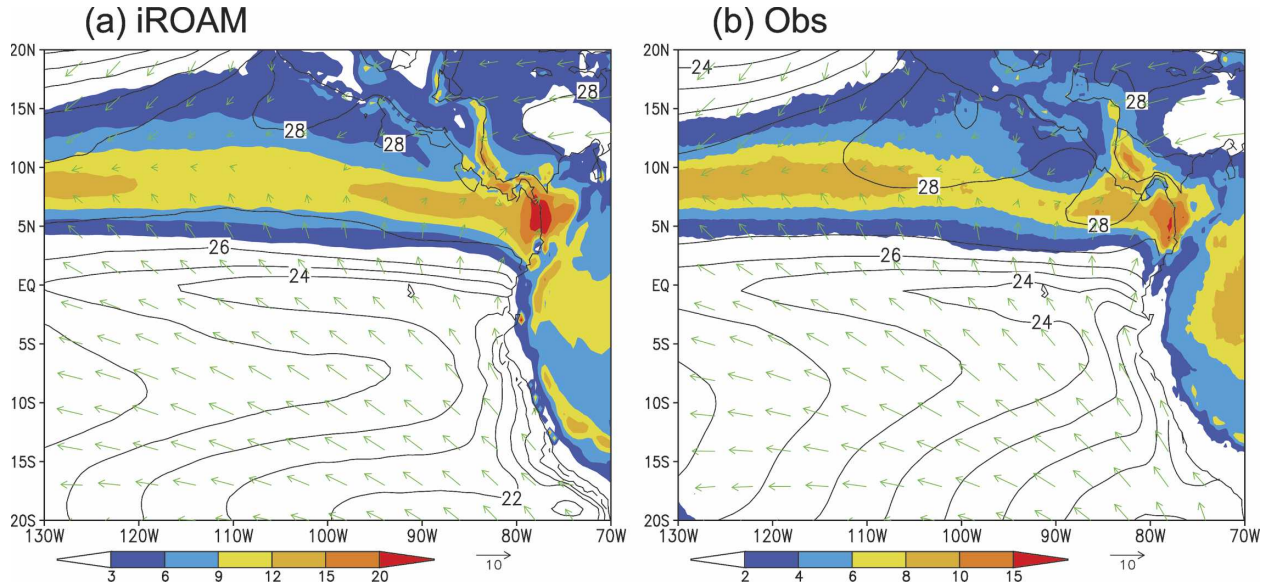


FIG. 3. Annual mean climatology of SST (contours in $^{\circ}\text{C}$), precipitation (color in mm day^{-1}), and surface wind velocity (m s^{-1}) in the (a) iROAM and (b) observations. Note the difference in color scale between (a) and (b).

band reaches all the way to Central America while strong upwelling develops off South America south of the equator. Philander et al. (1996) suggest that under the prevailing easterly trade winds, the southeast–northwest tilt of the coastal line of the tropical Pacific favors coastal upwelling south of the equator (Okajima et al. 2003). This asymmetry in coastal SST triggers coupled waves due to positive ocean–atmosphere feedback that propagates climatic asymmetry westward across the Pacific basin (Xie 1996; Ma et al. 1996; Xie and Saito 2001). The following wind–evaporation–SST (WES) feedback is at work to sustain latitudinal asymmetry over the Pacific (Xie and Philander 1994). Suppose that SST is slightly warmer north than south of the equator (say, due to asymmetry in coastal upwelling). The resultant pressure gradient drives southerly cross-equatorial winds, which veer eastward north (westward south) of the equator because of the Coriolis force, reducing (intensifying) the prevailing easterly trades. The wind-induced changes in surface evaporation reinforce the initial warming north and cooling south of the equator. Indeed, the southeast trades show a tendency to veer eastward north of the equator and wind speed is much weaker under the ITCZ than at similar latitudes south of the equator, in support of the WES feedback. Cloud interaction with the ocean is another important feedback, which will be discussed in section 3b.

In many coupled GCMs, the equatorial cold tongue tends to weaken east of the Galapagos toward the Ecuador coast. The iROAM equatorial cold tongue is quite realistic, with SST at its center decreasing mono-

tonically eastward and then connecting to the coastal upwelling zone south of the equator. This improved simulation of the equatorial cold tongue in the far eastern Pacific seems due to the realistic simulation of cross-equatorial southerlies, which are the major mechanism for sustaining the cold tongue east of 90°W by inducing upwelling slightly south of the equator. A climate of a stronger equatorial asymmetry features stronger cross-equatorial southerlies and more intense cooling near the equator. With reduced equatorial asymmetry and weak cross-equatorial southerlies, the simulated equatorial cold tongue may weaken in the far eastern Pacific (section 4a; see also Fig. 10 of Xie and Saito 2001) as in coupled models that suffer the double ITCZ syndrome.

a. Seasonal cycle

Figure 4 compares the monthly climatology between the iROAM and observations of SST, precipitation and surface wind velocity averaged over 120° – 100°W , as a function of latitude and time. The simulated seasonal cycle in the eastern Pacific is quite realistic. The model ITCZ stays north of the equator year-round, reaching its southernmost position in March and then marching northward until September in response to the increase in solar radiation and SST in the Northern Hemisphere. The seasonal excursion of the northern boundary of the ITCZ rainband is much more pronounced than the southern boundary, in agreement with observations. Remarkably the model captures the brief appearance

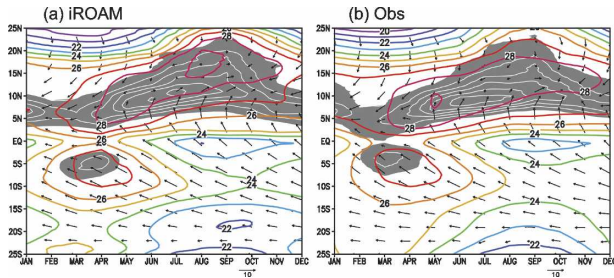


FIG. 4. Time-latitude sections of SST (color contours in °C), precipitation (gray shade > 2.5 mm day⁻¹ and white contours at 2.5 mm day⁻¹ intervals), and surface wind velocity (m s⁻¹) averaged in 120°–100°W for the (a) iROAM and (b) observations. Precipitation greater than 3.5 (2.5) mm day⁻¹ is shaded gray and contoured in white at 3.5 (2.5) mm day⁻¹ intervals in (a) and (b).

of a southern ITCZ from late February to early April when the Southern Hemisphere SST maximum exceeds 27°C in response to the seasonal increase in solar radiation in December–January. This symmetric double ITCZ was first observed from satellite cloud images by Kornfield et al. (1967) and revisited recently by Lietzke et al. (2001) and Zhang (2001). Overall, atmospheric deep convection follows the warmest water in the eastern Pacific, indicative of a strong SST control. This SST control is effective in the eastern Pacific presumably because high SSTs are confined in narrow zonal bands surrounded by high gradients.

The equatorial eastern Pacific features a pronounced annual cycle in SST and surface wind (Mitchell and Wallace 1992; Nigam and Chao 1996), a peculiar phenomenon inexplicable from local solar radiation that is dominated by a semiannual cycle. The iROAM reproduces the annual cycle on the equator quite well, in both amplitude and phase (Fig. 5). The warm phase takes place during March–April when the surface winds are weak. The annual maximum SST is about 1°C too cold compared to observations (26° versus 27°C). The warm season SST on the equator is sensitive to a number of factors, such as tropical Atlantic SST and Central American orography as will be discussed in section 4. Equatorial SST begins decreasing in April as surface winds intensify. The coldest phase takes place in August in the model, 1 month too early compared to observations. The annual minimum temperature is comparable with observations at about 21°C at 100°W. Consistent with observations, the wind velocity during the cold season is southerly east of 90°W, gains an easterly component to the west, and becomes nearly easterly at 140°W.

The northward-displaced ITCZ is the ultimate cause of the annual cycle in equatorial SST (Xie 1994). With the ITCZ staying north of the equator, cross-equatorial

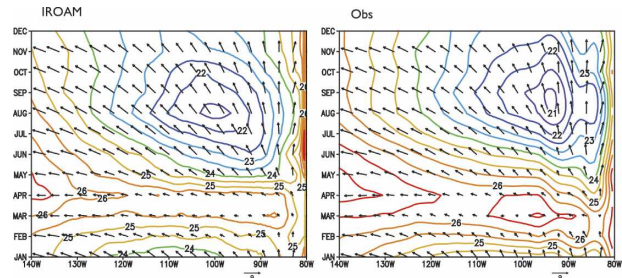


FIG. 5. Longitude-time sections of SST (color contours in °C) and surface wind velocity (m s⁻¹) on the equator for the (left) iROAM and (right) observations.

winds maintain their southerly direction but vary their speed in response to the seasonal cycle in solar radiation off the equator. Equatorial winds intensify in September when SST is at a maximum in the Northern Hemisphere and a minimum in the Southern Hemisphere and weaken in March when the seasonal cycle in off-equatorial SST reverses sign. This association of equatorial SST and wind is well simulated in the iROAM. Figure 6 shows the cold–warm seasonal differences in SST and surface wind. The agreement between the model and observations is remarkable. Largest wind differences between March and September are found north of the equator, associated with the seasonal migration of the ITCZ. Large SST differences, however, are found on and south of the equator because the shoaling thermocline there makes SST sensitive to wind changes. In September, the southeast trades intensify, cooling the equatorial SST by increasing the upwelling, vertical mixing, and surface evaporation. Along the equator, the easterly wind differences occupy the model domain west of 90°W in response to SST cooling that is larger toward the east. These easterly wind differences, in turn, drive upwelling on the equator and their interaction with SST causes a westward propagation of the annual cycle in both variables along the equator (Mitchell and Wallace 1992; Xie 1994; Nigam and Chao 1996).

Along the equator, the advance and retreat of the equatorial cold tongue are similar between the seasonal and interannual time scales, but this similarity is limited to SST. Figure 7 compares ocean temperature as a function of time and depth at 110°W, the equator between the iROAM simulation and Tropical Atmosphere Ocean (TAO) buoy. While the 1997/98 El Niño is associated with a large depression in the thermocline depth, the annual cycle in subsequent years is confined to the top 50 m within the surface mixed layer with little apparent seasonal cycle in the thermocline. Indeed, the 6-yr climatology confirms this surface confinement of the annual cycle. Temperature at 100 m has an annual

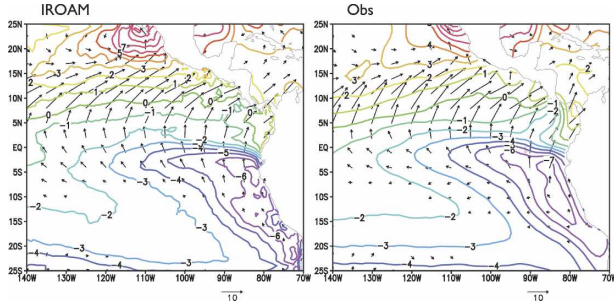


FIG. 6. September–March differences in SST (contours in $^{\circ}\text{C}$) and surface wind vectors (m s^{-1}) in (left) iROAM and (right) observations.

range of less than 1°C as opposed to more than 3°C at the sea surface (Figs. 7b,c). Compared to TAO observations the model thermocline is too diffuse, a common problem for GCMs, but the model reproduces the distinction in subsurface–surface coupling between the annual cycle and ENSO.

Figure 8 contrasts horizontal distributions of SST, precipitation, and surface wind between March and September, the warm and cold seasons for the equatorial and South Pacific. Eastern Pacific climate is nearly symmetrical in March, with one rainband in each hemisphere standing above warm SST on either side of the

equator, each separated from the other by cold SST along the equator. West of 120°W , the rainband and warm SST are closely collocated. East of 110°W , this collocation breaks, with the northern rainband displaced on the southern part of the eastern Pacific warm pool. This southward displacement of the rainfall maximum from the warm pool is noted by earlier observational studies (e.g., Hastenrath 1991) and is due to the orographic subsidence as the northeast trades impinge on Central American mountains (Xu et al. 2005). The iROAM simulates the cold patches over the Gulfs of Tehuntepec, Papagayo, and Panama, which result from wind jets through major gaps of the Central American mountain ranges (e.g., Xie et al. 2005). Both these gap wind jets and the resultant SST cooling are significantly weaker than observations because of insufficient resolutions to represent the narrow mountain ranges.

Strong asymmetry develops in September in the iROAM as in observations. The warm pool moves northward and occupies a broad meridional band toward Mexico, supporting strong precipitation. A sharp SST front develops north of the equator, near which the northward flow of cold upwelled water collides with the southward flow that carries warm water from the north (Raymond et al. 2004; de Szoeke et al. 2007). As in observations, the strongest upwelling cooling is found on the Peruvian coast at 15°S in both September and

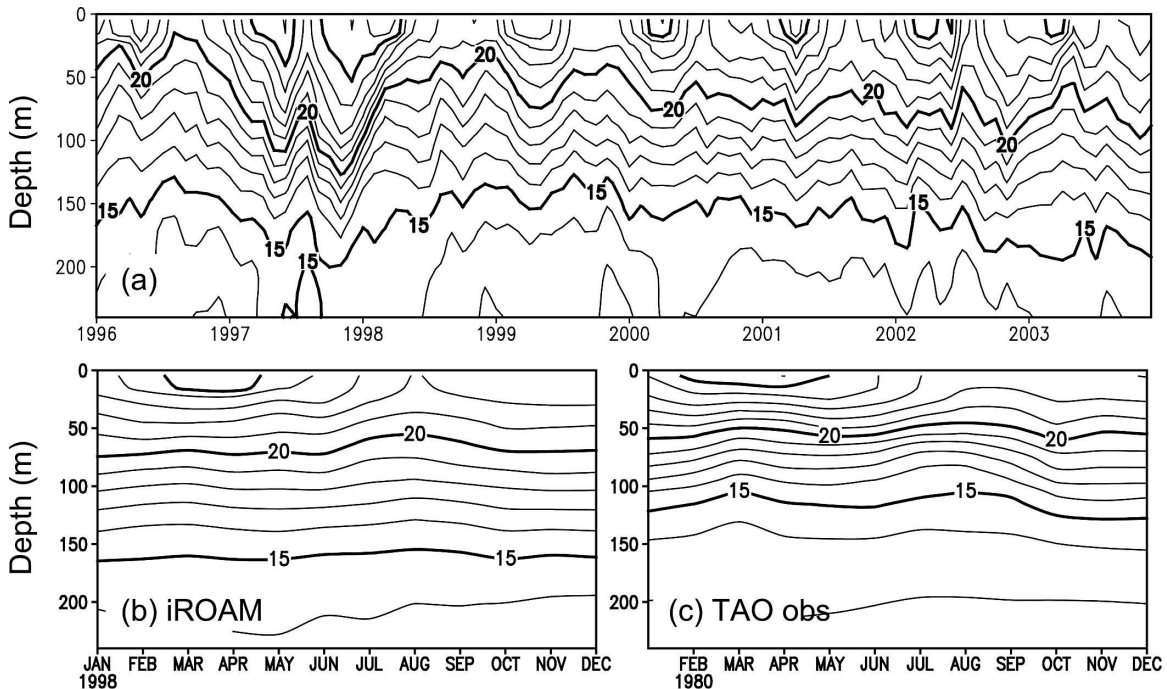


FIG. 7. (a) Time–depth section of ocean temperature ($^{\circ}\text{C}$) at 110°W , equator in the iROAM. Climatology for (b) iROAM and (c) TAO observations.

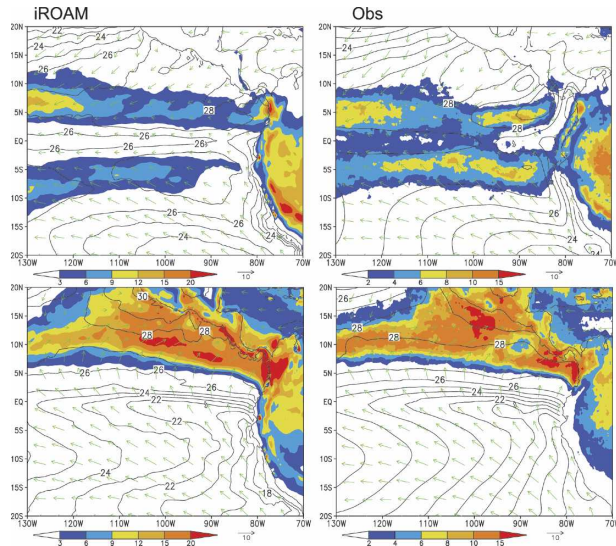


FIG. 8. (top) March and (bottom) September climatology of SST (black contours in $^{\circ}\text{C}$), precipitation (color shade in mm day^{-1}), and surface wind velocity (m s^{-1}) in the (left) iROAM and (right) observations. Note the difference in color scale between the left and right panels.

March where the slope of the coastline varies discontinuously.

b. Low cloud

Cloud is important for climate by modifying solar and longwave radiation both in the atmospheric column and at the surface. For example, the stratus cloud deck off the South American coast reduces the downward solar radiation by as much as 100 W m^{-2} in the annual mean (Fig. 9), from the clear sky value of about 300 W m^{-2} . In this paper we focus on the effect of cloud on surface shortwave radiation, as it is the most important for air–sea interaction. In the eastern Pacific, deep convective cloud and precipitation are in general positively correlated with SST, resulting in a negative feedback: an increase in SST leads to an increase in deep cloud and a reduction in shortwave radiation, which dampens the initial SST increase. Under the stratus cloud deck in the South Pacific, however, an SST increase reduces the lower-atmospheric stability and ABL cloud (Klein and Hartmann 1993), and the increased solar radiation amplifies the initial SST perturbation. Philander et al. (1996) show that this positive feedback between low cloud and SST is key to maintaining the latitudinal asymmetry of eastern Pacific climate.

Figure 9 compares the annual mean cloud cover between the iROAM and COADS. We define an effective cloud fraction as

$$C = (Q_{s0} - Q_{sc}) / (0.62Q_{s0}),$$

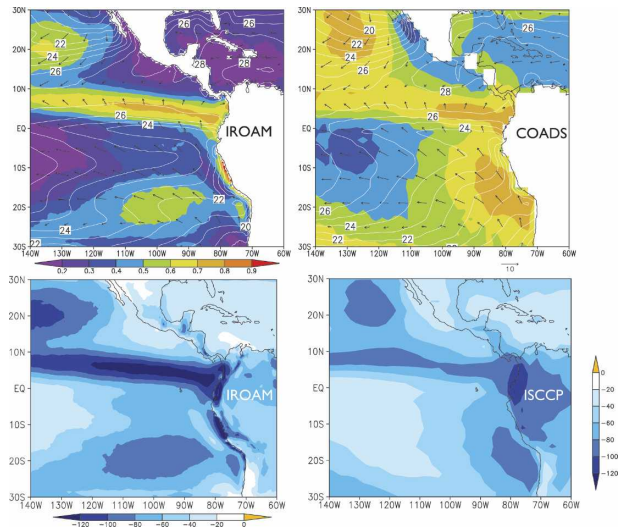


FIG. 9. (top) Annual mean cloudiness (color shade), SST (contours in $^{\circ}\text{C}$), and surface wind velocity (m s^{-1}) in the (left) iROAM simulation and (right) COADS observations. (bottom) Annual mean cloud radiative forcing (W m^{-2}) for downward shortwave radiation at the surface in (left) iROAM and (right) ISCCP observations.

based on the cloud effect on surface solar radiation, where Q_{sc} is the downward solar radiation at the sea surface and Q_{s0} is its clear-sky value. The factor of 0.62 is based on the empirical formula of Reed (1977) for surface solar radiation calculation using ship-based cloudiness observations. Thus, our effective cloudiness may be compared directly with COADS. We have also computed random overlapping cloudiness in the model and it is very similar to the above radiatively defined cloud cover. The model simulates the low-cloud decks over the subtropical North and South Pacific as well as a zonal cloud band centered near 5°N , which is a mixture of low cloud, shallow cumulus convection approaching the ITCZ, and deep convection in the ITCZ. The former frontal cloud forms as cold air moves from the equatorial cold tongue northward across the SST front (Wallace et al. 1989; Deser et al. 1993). The resultant boundary layer convection thickens the cloud as captured by recent field observations and model simulations (de Szoeke and Bretherton 2004; Small et al. 2005). Overall the simulated cloudiness is too low by 20% compared to COADS ship observations, but the cloud shortwave radiative forcing at the surface is quite comparable in magnitude to ISCCP observations, especially over the Southern Hemisphere. Thus radiative forcing appears to be slightly larger in surface (COADS) than satellite (ISCCP) observations.

The rest of this section focuses on the low-cloud deck off South America, whose shielding of solar radiation helps keep the South Pacific cool and maintains the

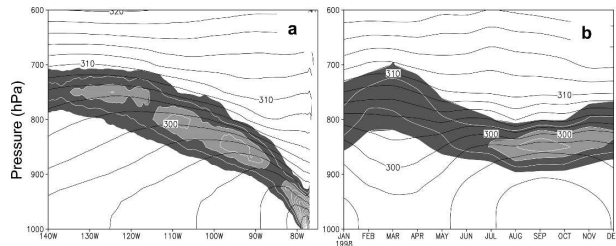


FIG. 10. Model cloud liquid water (shade $> 2 \times 10^{-2} \text{ g kg}^{-1}$ and white contours at $2 \times 10^{-2} \text{ g kg}^{-1}$ intervals) and virtual potential temperature (black contours in K) (a) along 12.5°S as a function of longitude and pressure and (b) at 12.5°S , 95°W as a function of time and pressure.

climatic asymmetry across the equator. Both the cold sea surface and strong subsidence are important for the formation of this cloud deck. The subsidence,¹ partly forced by the rising motion in the ITCZ north of the equator, warms the free troposphere and a temperature inversion forms separating the warm troposphere from the cold ocean surface. The inversion traps moisture, under which cloud forms. The cloud-top longwave radiation reinforces the inversion and cloud formation by cooling the cloud and encouraging ABL turbulence. The South Pacific cloud deck in the model is somewhat confined in the subtropics instead of extending to near the equator in COADS and has too small a cloud fraction. The cloud deficit is especially large near the coast. (Very near the coast, the model maintains a high fraction of cloud because of a larger number of cloud condensation nuclei there.)

Figure 10a displays the vertical structure of the South Pacific cloud deck along 12.5°S as a function of longitude. East of 100°W , cloud forms at the top of the mixed layer as turbulence mixes surface air above the lifting condensation level. In such a coupled ABL, the cloud is coupled directly with the sea surface via turbulent mixing (e.g., Bretherton and Wyant 1997). On the coast, the upwelling cooling is so intense that there is no mixed layer with cloud touching the sea surface. As SST increases west of 100°W , the cloud base is decoupled from the mixed layer and separated by a stably stratified layer. In such a decoupled ABL, shallow cumulus convection transports vapor and liquid water through the stable layer and detrains when its vertical development is inhibited by the inversion. Observations of cloud vertical structure are scarce in the South Pacific (Bretherton et al. 2004). Based on a cruise sur-

vey along 27°S , Garreaud et al. (2001) report a zonal transition from a shallow, well-mixed ABL topped by stratocumulus near the coast to a deeper, decoupled ABL with cumulus rising into a patchy stratocumulus cloud deck near 110°W in support of the simulated cloud regime transition. We note that Garreaud et al.'s transect is located farther to the south and the simulated cloud-top temperature needs to be compared with satellite observations for verification.

Because SST varies in both space and time, a similar cloud regime transition is found in simulated cloud over the course of the seasonal cycle. Figure 10b shows cloud structure as a function of time and height at 12.5°S , 95°W . During the cold season (August–October), SST is low and cloud is in the coupled regime forming above the mixed layer. During the warm season (February–April), SST warms up and the cloud base is decoupled from the mixed layer by a stable layer (900–825 hPa). We are not aware of direct observations of such cloud regime transition in time in response to the SST seasonal cycle, but it is a good target for future field observations.

The cloud regime transition is considered important for cloudiness variations (Norris 1998). In the coupled ABL, stratus and stratocumulus clouds are largely unbroken in space as observed near the South American coast. In the decoupled ABL, cumulus clouds are organized in space and occupy a small fraction of the sky. Upon reaching the inversion, the cumulus plume entrains dry air from the inversion layer, evaporating cloud droplets and dissipating the cloud. As a result, the cloud cover is generally greater for coupled than uncoupled clouds (Albrecht et al. 1995; Yuter et al. 2000). Indeed, the seasonal cycle in cloudiness in our model is associated with cloud regime transition. Visual examination of cloud water at 12.5°S , 95°W (Fig. 10b) indicates that the coupled clouds during August–October are optically thicker than the decoupled clouds during February–March.

Figure 11 compares cloudiness in the eastern Pacific between the iROAM and observations. Between the equator and 20°S , cloudiness is high during the cold season and low during the warm season except in a narrow latitudinal band where the southern ITCZ briefly appears. The model captures this general seasonal cycle in cloud. In both the model and COADS, the cloud band north of the equator weakens in March as both the northern ITCZ and cross-SST frontal advection weaken. The fraction of this cloud band increases during the boreal summer and fall when both the ITCZ and the southerly cross-frontal flow intensify. Overall, the eastern Pacific (including the equator) is cloudier in September than March, contributing to the

¹ The subsidence at 700 mb is 30%–60% stronger than in the NCEP reanalysis because of the aforementioned excessive precipitation in the ITCZ (Fig. 3) and too strong a hydrological cycle in the model.

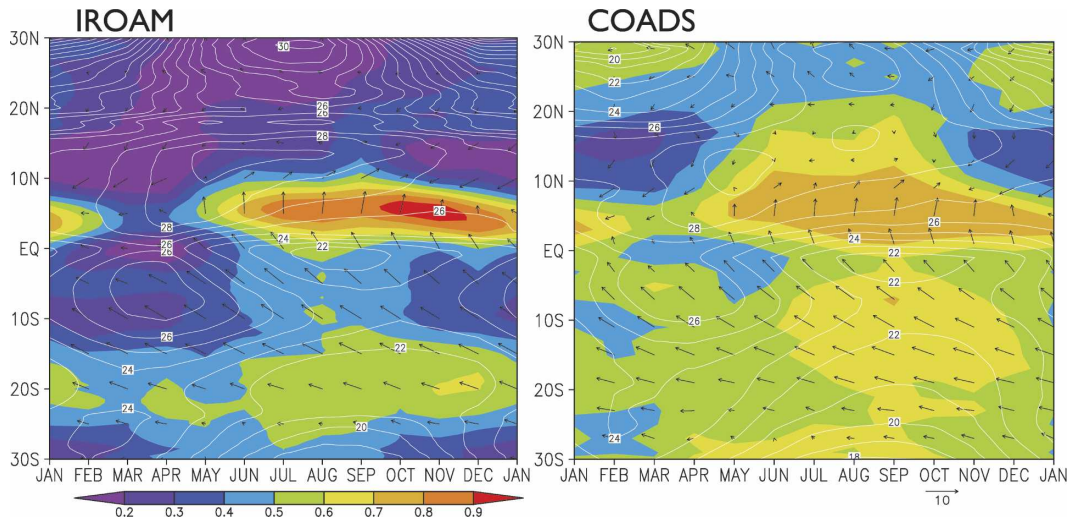


FIG. 11. Time-latitude sections of cloudiness (color shade), SST (contours), and surface wind velocity, all averaged in 110° – 90° W in the (left) iROAM simulation and (right) COADS observations.

annual cycle in equatorial SST (Kessler et al. 1998; Yu and Mechoso 1999).

4. Sensitivity experiments

The atmospheric component of the iROAM is forced by the reanalysis on the lateral boundaries and by observed SST over the Atlantic, while the ocean component is forced in the western basin by the wind stress and heat flux computed by bulk formulas from the NCEP–NCAR reanalysis. One may question if the realism of the simulation is trivial, set a priori by these external forcings. We have carried out a number of experiments to test the sensitivity to forcing and internal feedbacks. The results show that internal air–sea feedbacks are very important for a realistic simulation. This section presents two examples, one to investigate the sensitivity to the cloud feedback and one to the Atlantic SST.

a. Cloud feedback

In the southeast Pacific (east of 110° W, equator to 30° S), the low-cloud deck reduces surface solar radiation by 50 – 100 W m^{-2} in the model depending on location (Fig. 9), an important cooling for the hemispheric asymmetry in SST. We carry out an experiment by removing cloud effects on radiation (both short- and longwave) south of the equator (No-CRF-SH run). This removal of cloud radiative forcing increases the annual mean SST by 2° – 3° C between the equator and 20° S (Fig. 12a versus Fig. 3a), nearly destroying the hemispheric asymmetry in SST.

Figure 12b shows the seasonal cycles of SST, precipitation, and surface wind as a function of time and latitude. The southern rainband first appears in December and persists for half a year through June. In March, SST south of the equator exceeds 30°C , more than 2°C above the SST maximum at the same time in the Northern Hemisphere. This reversed asymmetry is so large that it eliminates the northern rainband. In addition to solar radiation, the WES feedback is also involved in creating this reversed latitudinal asymmetry. During January–May, surface winds converge onto the Southern Hemisphere and strong northeasterlies cool SST via evaporation north of the equator while winds are weak over the warm water band in the Southern Hemisphere. The northern rainband begins to recover in April and gradually intensifies through August–September as solar radiation and SST increase north and decrease south

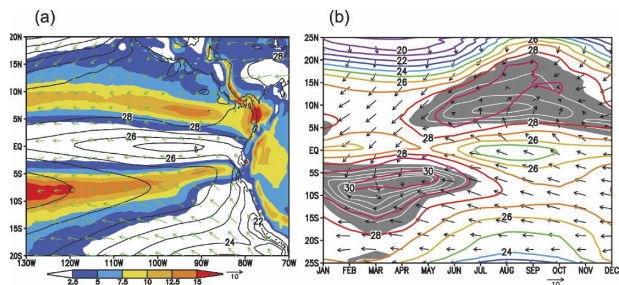


FIG. 12. (a) Annual mean climatology of SST (contours in $^{\circ}\text{C}$), precipitation (color shade mm day^{-1}), and surface wind velocity in an experiment where cloud radiative effects are removed south of the equator. (b) Same as (a) but averaged in 120° – 100° W as a function of time and latitude (with precipitation > 5 mm day^{-1} shaded and contoured at 5 mm day^{-1} intervals).

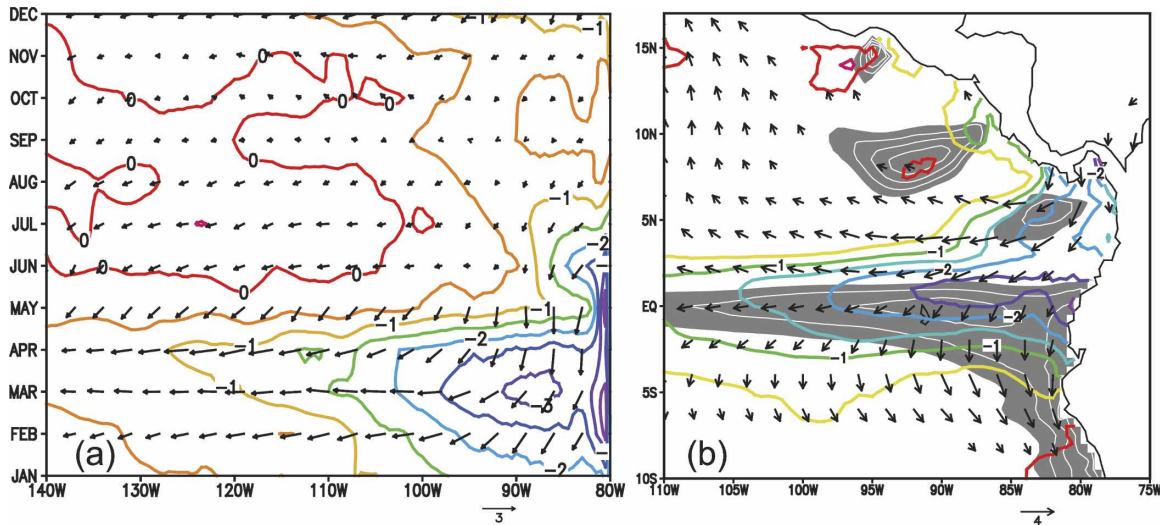


FIG. 13. SST (color contours) and surface wind velocity differences from the control in an experiment where North Atlantic SST is reduced by 2°C. (a) At the equator as a function of longitude and time and (b) horizontal distributions in March. Also plotted in (b) is ocean temperature in total field at 35 m (white contours with shade < 24°C at 1°C intervals).

of the equator. To first order, the ITCZ moves back and forth across the equator following the sun in this No-CRF-SH run, a seasonal cycle observed in the western tropical Pacific. The cross-equatorial wind changes direction and as a result, equatorial SST acquires a semiannual cycle while weakening its annual cycle.

Thus, the removal of cloud radiative effects in the Southern Hemisphere pushes the iROAM into the double ITCZ syndrome seen in many global coupled GCMs. This experiment also demonstrates that the external forcing is insufficient to guarantee a realistic simulation and that internal air–sea feedback is crucial. Y. Wang et al. (2005) carry out an identical experiment with the iRAM that prescribes observed SST. Low cloud almost disappears without cloud radiative effects (especially the cloud-top cooling), but the response of dynamical fields is quite modest with fixed SST. With an interactive SST in iROAM, the cloud effect on surface solar radiation becomes dominant and dramatically alters Pacific climate, consistent with previous studies (Philander et al. 1996; Ma et al. 1996; Yu and Mechoso 1999; Gordon et al. 2000).

In the No-CRF-SH run, the annual mean rainfall distribution becomes nearly symmetric about the equator throughout the model domain, but significant asymmetry remains in SST east of 110°W, with the northern SST maximum greater than the southern one. Strikingly, the hemispheric asymmetry in coastal upwelling remains strong, with cold SST on the South American coast. Latitudinal asymmetry may be considered as being forced by continental geometry with the help of air–sea feedback that propagates the continental forc-

ing westward (Xie 1996). With the air–sea feedback reduced (by removing the SST–cloud feedback in the Southern Hemisphere in the No-CRF-SH run) the westward development of latitudinal asymmetry is greatly reduced despite the same land–sea distribution.

The importance of internal feedbacks in shaping the regional model climate is not very surprising given the large domains used by the iROAM components. While this and many GCM studies emphasize the SST–low-cloud interaction, other air–sea feedbacks are also important for climatic asymmetry about the equator. For example, west of 100°W the annual mean cloudiness is greater north than south of the equator (Fig. 9) in favor of a warmer Southern Hemisphere, but the high SST band and ITCZ remain in the Northern Hemisphere. Other feedbacks, such as WES, must operate to sustain these asymmetries far into the west (Xie and Philander 1994; Xie 1996).

b. Atlantic influence

The second experiment explores the sensitivity to tropical Atlantic SST and investigates how changes in the Atlantic are communicated to the tropical Pacific, a topic of important paleoclimatic implications (Timmermann et al. 2007) as will become clear. For simplicity, we decrease Atlantic SST by 2°C north of 5°N and taper this change off over 5°N–5°S. The Pacific response is highly seasonal. On the equator, considerable cooling of up to 3°C takes place during January–April, the largest in the east and gradually decaying in 120°–90°W (Fig. 13a). Figure 13b shows the response of SST

and surface wind to the North Atlantic cooling in March. Large SST anomalies are found on the equator because of the Bjerknes feedback: the SST cooling in the east drives anomalous easterlies, which reinforces the cooling by enhancing equatorial upwelling and shoaling the thermocline. The cooling can be traced back to the Gulf of Panama.

Atlantic cooling increases the sea level pressure by about 2 hPa in the Caribbean Sea (not shown), intensifying the gap winds in the Gulf of Panama. December–April happen to be the time when the mean Panama gap wind jet develops, shoaling the thermocline underneath with the positive wind curl on the jet's southeast flank (gray shade and white contours in Fig. 13b; see Xie et al. 2005 for observations). This thermocline ridge shoals further in response to equatorial easterlies induced by Atlantic cooling, resulting in a 4°C cooling at a 35-m depth (not shown). This anomalous shoaling of the thermocline is roughly collocated with SST cooling. Evaporative cooling also increases over the thermocline ridge as the Panama wind jet intensifies and advects colder/drier air from the Caribbean. (This increased dry advection causes a southward displacement of the ITCZ.) Thus, the existence of the wind jet and thermocline ridge in the Gulf of Panama makes January–April the favored season for large Gulf of Panama SST response. This Gulf of Panama cooling extends southwestward, triggering the Bjerknes feedback for amplification along the equator. The Panama wind jet weakens and disappears from April onward, cutting off this link between the Caribbean and equatorial Pacific. The seasonality of Atlantic-induced cooling in Fig. 13a corresponds to a reduced annual cycle in eastern equatorial Pacific SST.

ENSO's influence on the tropical North Atlantic is well known, a warming taking place in the latter during March–May following the peak warming in the eastern Pacific via atmospheric teleconnection (e.g., Enfield and Mayer 1997). Possible Atlantic influence on the Pacific is receiving increasing attention in the context of studying the Younger Dryas of 11 000 yr before present, a large and rapid cooling event believed to originate from the high-latitude North Atlantic as the remnants of the Laurentide ice sheet melted into the sea and shut down the thermohaline circulation (THC). The tropical Atlantic response to such a large cooling in the high-latitude North Atlantic is quite consistent among the models, with cooling north and slight warming south of the equator as a result of the WES feedback (Chiang et al. 2003; Wu et al. 2005; Timmermann et al. 2007). The Pacific SST response is more diverse among the models, ranging from a permanent El Niño (Dong and Sutton 2002; Wu et al. 2005) to a meridional

dipole across the equator (Zhang and Delworth 2005). Our model results suggest that the Pacific response to North Atlantic changes is sensitive to the treatment of narrow Central American mountains, a geographical feature poorly represented in global GCMs of 2.5° or coarser resolutions, on which all the above studies are based. In particular, we suggest that the Panama wind jet, a result of orographic forcing, serves as a key link in communicating the Atlantic change to the equatorial Pacific.

5. Mesoscale features

Relatively high resolution of our regional model affords the study of mesoscale phenomena in the ocean and atmosphere, which are generally not adequately represented in global GCMs. This section illustrates this utility with two examples: the Costa Rica Dome west of Central America and tropical instability waves (TIWs). In an independent study using a different ROAM, Seo et al. (2007) also successfully simulate ocean–atmospheric covariability in TIWs and the Costa Rica Dome.

a. Costa Rica Dome and Tsuchiya Jet

In boreal winter, sea level pressure in the Caribbean exceeds that in the tropical Pacific, and three wind jets develop in the Gulfs of Tehuantepec, Papagayo, and Panama as air rushes down the pressure gradient through gaps in the Central American mountains. The synoptic development (Chelton et al. 2000) and climatological distribution (Xie et al. 2005) of these jets are recently mapped from satellite observations. The iROAM reproduces these wind jets and the attendant SST patterns (Fig. 14a)—cold patches under the jets and warm patches in between—but with reduced sharpness compared to observations. The Panama jet tilts too much toward the west in the model, which is nearly meridional in observations (Fig. 6 of Xie et al. 2005). The strong wind curls of the jets imprint on the thermocline topography, including a pronounced ridge southwest of each of the Papagayo and Panama jets (gray shade and white contours in Fig. 13b). In the Gulf of Panama the thermocline ridge dissipates quickly as the ITCZ moves northward and the wind jet disappears. The ridge southwest of Papagayo is called the Costa Rica Dome and a permanent feature of the thermocline, partly because the nearly zonal orientation of the wind jet allows ocean Rossby waves to propagate far and partly because of the positive wind curls during summer when the ITCZ is overhead. The model captures this thermocline dome centered at 9°N, 90°W as

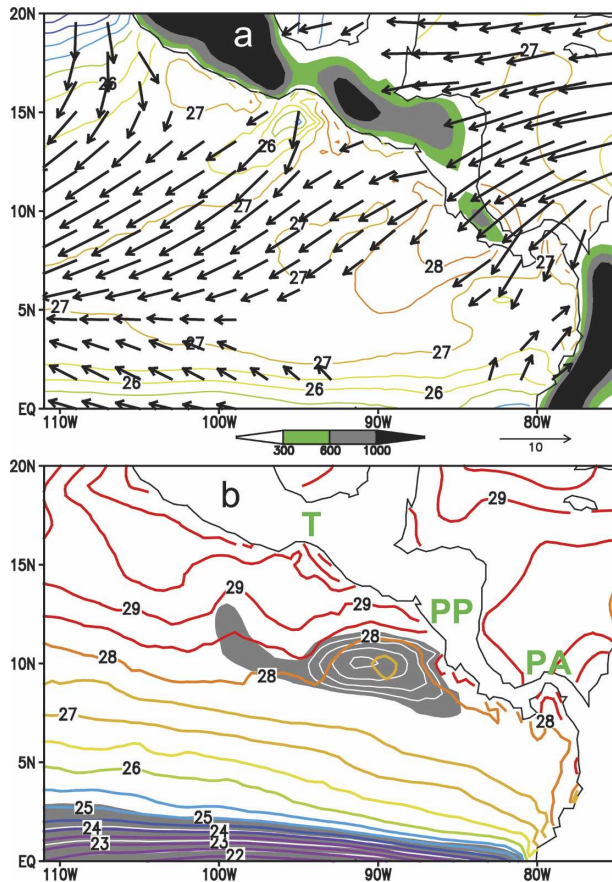


FIG. 14. (a) Surface wind vectors (m s^{-1}) and SST ($^{\circ}\text{C}$) for February–March, along with land orography (m). (b) Ocean temperature at the surface (color contours in $^{\circ}\text{C}$) and 35 m (white contours with shade $< 25^{\circ}\text{C}$) for July–August. Major mountain gaps are marked in (b): Tehuantepec (T), Papagayo (PP), and Panama (PA).

well as the cool spot in SST over the dome in summer (Fig. 14b). The near collocation of the dome and cool spot in SST suggests that the entrainment of cold thermocline water is the cause of the latter. In observations, this cool spot punches a conspicuous hole of a 500-km radius in the summer ITCZ rainband (Xie et al. 2005), a feature not easily identifiable in the model.

The summer cool spot at the surface is a signature of persistent upwelling in the Costa Rica Dome. Kessler (2002) suggests that this upwelling is an important element of intermediate water circulation in the Pacific. Indeed, McCreary et al.'s (2002) numerical study demonstrates that the upwelling in the dome drives an eastward subsurface current north of the equator called the Tsuchiya jet by causing characteristics of different potential vorticity to meet. Figure 15 shows the zonal current velocity and temperature in a meridional transect along 110°W . The model reproduces quite well the ma-

ajor equatorial currents, including the South Equatorial Current, Equatorial Undercurrent (of maximum velocity $> 1 \text{ m s}^{-1}$), and the North Equatorial Countercurrent (NECC). In particular, the model features a narrow subsurface eastward jet with the maximum speed of 15 cm s^{-1} centered around 4°N in a depth range of 100–300 m displaced equatorward of the surface NECC. As in observations, this model's Tsuchiya jet is associated with a potential vorticity front in the lower thermocline with a rapid northward increase in potential vorticity. The link between the Costa Rica Dome upwelling and Tsuchiya jet is suggested by an experiment that flattens Central American mountains. In this experiment, both the upwelling in the Costa Rica Dome and the Tsuchiya jet weakens (not shown).

b. Tropical instability waves

During the second half of the year, the equatorial front often produces cusp-shaped meanders (Legeckis 1977; Wentz et al. 2000) due to the hydrodynamic instabilities of sheared equatorial currents. Early buoy observations (Hayes et al. 1989) indicate surface wind covariability with these TIWs, an association confirmed from satellite observations (Xie et al. 1998). The 1999 TIW season coincides with the launch of the QuikSCAT satellite, stirring much interest in mapping this ocean–atmospheric covariability from space (Liu et al. 2000; Chelton et al. 2001; Hashizume et al. 2001). The year 1999 also marks the first time that TIW variability is profiled simultaneously in the ocean and atmosphere on board a ship (Hashizume et al. 2002).

The iROAM captures TIWs and their statistical properties. Figure 16b shows the longitude–time section for 1999 of SST and surface wind convergence at 2°N , a latitude where TIWs are large in amplitude. SST waves are $2^{\circ}\text{--}4^{\circ}\text{C}$ in peak-to-trough amplitude, about monthly in period, and 10° in wavelength in agreement with observations. Clear copropagation is seen between SST and wind divergence. As Chelton et al. (2001) observe from QuikSCAT, enhanced wind divergence is located to the west of the SST cusps as wind accelerates across the SST front toward warmer water (Fig. 16a). The prevailing southeasterlies strengthen over the warm and weaken over the cold phase of TIWs as in observations (not shown). These wind anomalies tend to converge (diverge) into centers of low (high) sea level pressure that are displaced downwind of centers of SST anomalies, as in Small et al.'s (2003) iRAM simulation forced by observed SST. TIWs are an important mechanism for distributing heat in the meridional direction (e.g., Jochum and Murtugudde 2006) and the iROAM offers a tool to study how their interaction

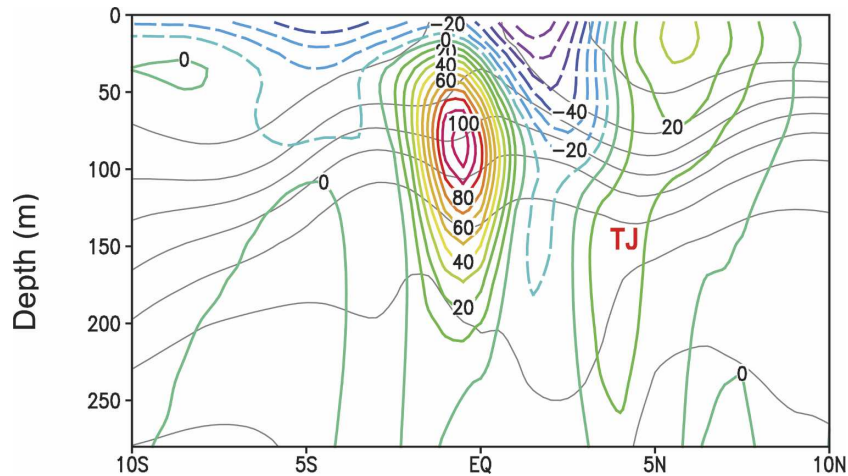


FIG. 15. Annual mean zonal current velocity (color contours in cm s^{-1}) and temperature (thin gray contours in $^{\circ}\text{C}$ with 2°C intervals) at 110°W in the iROAM simulation.

with the atmosphere affects this meridional heat transport.

6. Summary

We have constructed a regional coupled ocean–atmosphere model and tested it over the eastern tropical Pacific. The model reproduces salient features of eastern Pacific climate on both the basin and meso-scales. In particular, it succeeds in keeping the ITCZ north of the equator throughout the year, an important hemispheric asymmetry that many global coupled GCMs have difficulty simulating (Mechoso et al. 1995). The model ITCZ is displaced north of the equator for a brief period of late February–April when the Southern Hemisphere warms up, tropical SST becomes nearly symmetric, and a double ITCZ appears astride the equator, all in agreement with observations. A pronounced annual cycle appears in equatorial SST in association with annual variations in cross-equatorial wind that maintains its southerly direction year-round converging onto the northward-displaced ITCZ. As in observations, this annual cycle is trapped in the ocean mixed layer, with little vertical displacement of the thermocline unlike ENSO. By contrast thermocline displacement is of first-order importance for ENSO. Such a realistic simulation is not solely due to the use of observations to force the model on open boundaries. Our sensitivity experiments demonstrate that internal feedbacks between the ocean and atmosphere are essential to maintain climatic asymmetry across the equator.

The extensive low cloud over the southeast Pacific is an important mechanism for keeping SST low there. The iROAM reproduces this cloud deck but at reduced

cloudiness. Eliminating the radiative effects of this cloud deck in the Southern Hemisphere results in a nearly symmetric annual mean climate over the eastern Pacific, with the ITCZ moving back and forth across the

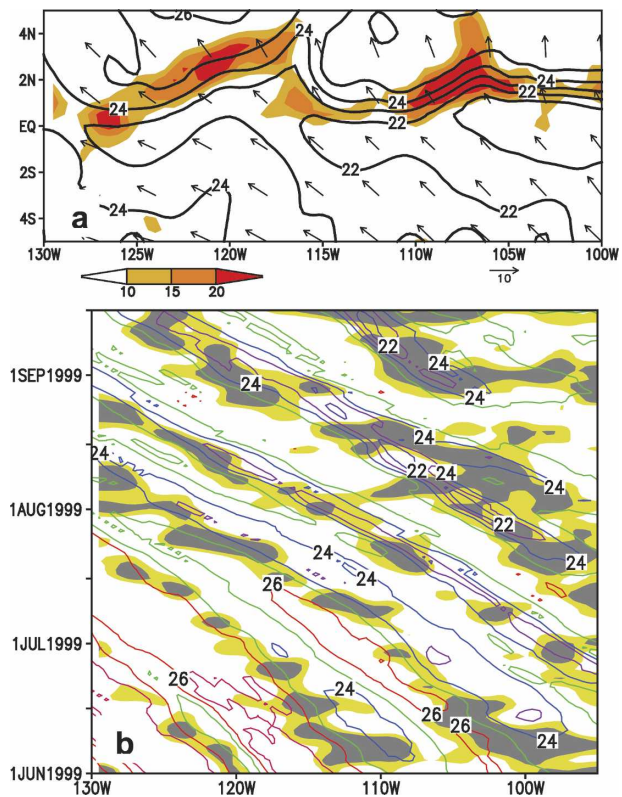


FIG. 16. (a) SST (contours in $^{\circ}\text{C}$), surface wind velocity (vectors in m s^{-1}), and divergence (color in 10^{-6} s^{-1}). (b) Longitude–time section of SST ($^{\circ}\text{C}$) and surface wind divergence (yellow shade > 7 and gray shade $> 10 \times 10^{-6} \text{ s}^{-1}$) along 2°N . A 3-point running mean has been applied 3 times both in longitude and time in (b).

equator following the sun. The control run successfully simulates the cloud regime transition in space and time. In a given season, stratiform cloud forms in a coupled ABL near the South American coast and the cloud base gradually rises and becomes decoupled from the surface mixed layer as SST increases toward the west. Cloud in the decoupled ABL is supported by moisture transport by shallow cumulus convection, which rises through the stable layer between the mixed-layer top and cloud base. Such a cloud regime transition occurs in the seasonal cycle as well: stratiform cloud forms in a coupled ABL in September, while it becomes decoupled in March when the ocean warms up. This cloud regime transition is associated with cloudiness changes, with reduced cloudiness in the decoupled ABL during the warm season. Future observations are necessary to test this model-based hypothesis of the seasonal transition in cloud regime in the southeast Pacific.

ENSO is the most important mode of climate variability in the instrumental record because of strong air–sea interaction in the tropical Pacific. Paleoclimate records indicate that the interaction of the North Atlantic thermohaline circulation and ice sheets is important for variability on centennial or longer time scales. Our model results suggest that the wind jet and resultant upwelling in the Gulf of Panama serve as an important link for Atlantic changes to influence the tropical Pacific. In response to a decrease in North Atlantic SST, equatorial Pacific SST decreases by a comparable or greater amount in January–April, but its change is much smaller in other seasons, resulting in a decrease in the amplitude of the equatorial annual cycle. Such a possible modulation of the Atlantic-to-Pacific influence by Central America needs to be further explored with models that resolve the narrow mountains on the land bridge. Such studies are important to understand the global climate response to a thermohaline circulation shutdown, such as during the Younger Dryas event, given the strong interaction of ENSO and equatorial annual cycle and possible Pacific feedback onto the North Atlantic via atmospheric teleconnections.

Increased model resolution improves the representation of mesoscale features in the ocean, atmosphere, and land. The iROAM simulates monthly TIWs along the equatorial front that induce the surface wind fluctuations with realistic amplitude, period, and wavelength. It reproduces the gap wind jets off the west coast of Central America and the permanent thermocline dome off Costa Rica. To our knowledge the iROAM is the first coupled model that simulates the Tsuchiya Jet, centered at 4°N with a speed of 15 cm s⁻¹. This subsurface current is associated with a potential

vorticity front in the lower thermocline, flowing eastward toward the Costa Rica Dome. Experiments to be presented elsewhere indicate that narrow mountains of Central America have a significant effect on this basin-wide ocean jet.

The iROAM shows skills in simulating the climatology of the eastern Pacific in contrast to the more typical performance of global coupled GCMs with reduced climatic asymmetry and a cold tongue that is too cold and displaced too far west (Mechoso et al. 1995). The iROAM may contribute to reducing these biases by acting as a test bed for comparison with other models and sensitivity experiments. This paper shows that shortwave modulation by low cloud is an important physical process to simulate a realistic asymmetry. We have performed iROAM experiments to explore the sensitivity to shallow cumulus convection and drizzle parameterizations and showed that they are important for the southeast Pacific low-cloud deck and the basin-scale meridional asymmetry (de Szoeke et al. 2006). Sensitivity to model resolution is another issue relevant to global model development and interpretation. Horizontal resolution affects coastal winds and upwelling while vertical resolution may influence cloud-top entrainment. To facilitate comparison with other models, the control run output is available online at http://www.jamstec.go.jp/frcgc/k7-dbase2/search_e/datadoc/iROAM.html on the World Wide Web.

The iROAM shows high skills in simulating atmospheric intraseasonal variability (not shown), which is forced on the iRAM's lateral boundaries. The correlation of 850-mb zonal wind on the equator between the simulation and observations amounts to 0.5 in the intraseasonal frequency band for the 6-yr period of 1998–2003, far exceeding the 95% significance level. Given the persisting difficulty global GCMs have in simulating the Madden–Julian oscillation (Lin et al. 2006), the iROAM is potentially a useful tool to study regional features of this dominant mode of tropical convection and its interaction with the ocean.

Acknowledgments. We wish to thank T. Li for helping configure MOM2, J. Hafner and Y. Zhang for data preparation, Z. Yu and R. Furue for helpful discussion, and K. Horiuchi and Y. Shen for maintaining the OpenDAP server in Yokohama through which the model output is analyzed. Most of the computation is carried out on the Earth Simulator, Yokohama, Japan. This work is supported by the Ministry of Education, Culture, Science and Technology through the Kyosei-7 Project, the U.S. National Oceanic and Atmospheric Administration, the U.S. National Aeronautics and Space Administration, and the Japan Agency for Ma-

rine-Earth Science and Technology. T. M., Y. W., and H. X. contribute equally.

REFERENCES

- Albrecht, B. A., C. S. Bretherton, D. Johnson, W. H. Schubert, and A. S. Frisch, 1995: The Atlantic Stratocumulus Transition Experiment—ASTEX. *Bull. Amer. Meteor. Soc.*, **76**, 889–904.
- Bretherton, C. S., and M. C. Wyant, 1997: Moisture transport, lower-tropospheric stability, and decoupling of cloud-topped boundary layers. *J. Atmos. Sci.*, **54**, 148–167.
- , and Coauthors, 2004: The EPIC 2001 stratocumulus study. *Bull. Amer. Meteor. Soc.*, **85**, 967–977.
- Chang, P., B. Wang, T. Li, and L. Ji, 1994: Interactions between the seasonal cycle and the Southern Oscillation-frequency entrainment and chaos in a coupled ocean–atmosphere model. *Geophys. Res. Lett.*, **21**, 817–820.
- Chelton, D. B., M. H. Freilich, and S. K. Esbensen, 2000: Satellite observations of the wind jets off the Pacific coast of Central America. Part I: Case studies and statistical characteristics. *Mon. Wea. Rev.*, **128**, 1993–2018.
- , and Coauthors, 2001: Observations of coupling between surface wind stress and sea surface temperature in the eastern tropical Pacific. *J. Climate*, **14**, 1479–1498.
- Chiang, J. C. H., M. Biasutti, and D. S. Battisti, 2003: Sensitivity of the Atlantic ITCZ to conditions during Last Glacial Maximum. *Paleoceanography*, **18**, 1094, doi:10.1029/2003PA000916.
- Deser, C., S. Wahl, and J. J. Bates, 1993: The influence of sea surface temperature gradients on stratiform cloudiness along the equatorial front in the Pacific Ocean. *J. Climate*, **6**, 1172–1180.
- de Szoeke, S. P., and C. S. Bretherton, 2004: Quasi-Lagrangian large eddy simulations of cross-equatorial flow in the east Pacific atmospheric boundary layer. *J. Atmos. Sci.*, **61**, 1837–1858.
- , Y. Wang, S.-P. Xie, and T. Miyama, 2006: The effect of shallow cumulus convection on the eastern Pacific climate in a coupled model. *Geophys. Res. Lett.*, **33**, L17713, doi:10.1029/2006GL026715.
- , S.-P. Xie, R. J. Small, and T. Miyama, 2007: What maintains the SST front north of the eastern Pacific equatorial cold tongue? *J. Climate*, in press.
- Dickinson, R. E., A. Henderson-Sellers, and P. J. Kennedy, 1993: Biosphere–Atmosphere Transfer Scheme (BATS) version 1e as coupled to the NCAR Community Climate Model. NCAR Tech. Note NCAR/TN-387+STR, 72 pp.
- Dijkstra, H. A., and J. D. Neelin, 1995: Ocean–atmosphere interaction and the tropical climatology. Part II: Why the Pacific cold tongue is in the east. *J. Climate*, **8**, 1343–1359.
- Dong, B.-W., and R. T. Sutton, 2002: Adjustment of the coupled ocean–atmosphere system to a sudden change in the thermohaline circulation. *Geophys. Res. Lett.*, **29**, 1728, doi:10.1029/2002GL015229.
- Edwards, J. M., and A. Slingo, 1996: Studies with a flexible new radiation code. I: Choosing a configuration for a large-scale model. *Quart. J. Roy. Meteor. Soc.*, **122**, 689–719.
- Enfield, D. B., and D. A. Mayer, 1997: Tropical Atlantic SST variability and its relation to El Niño–Southern Oscillation. *J. Geophys. Res.*, **102**, 929–945.
- Fairall, C. W., E. F. Bradley, D. P. Rogers, J. B. Edson, and G. S. Young, 2003: Bulk parameterization on air–sea fluxes: Updates and verification for the COARE algorithm. *J. Climate*, **16**, 571–591.
- Garreaud, R. D., J. Rutllant, J. Quintana, J. Carrasco, and P. Minnis, 2001: CIMAR–5: A snapshot of the lower troposphere over the subtropical southeast Pacific. *Bull. Amer. Meteor. Soc.*, **82**, 2193–2207.
- Gordon, C. T., A. Rosati, and R. Gudgel, 2000: Tropical sensitivity of a coupled model to specified ISCCP low clouds. *J. Climate*, **13**, 2239–2260.
- Hashizume, H., S.-P. Xie, W. T. Liu, and K. Takeuchi, 2001: Local and remote atmospheric response to tropical instability waves: A global view from the space. *J. Geophys. Res.*, **106**, 10 173–10 185.
- , —, M. Fujiwara, M. Shiotani, T. Watanabe, Y. Tanimoto, W. T. Liu, and K. Takeuchi, 2002: Direct observations of atmospheric boundary layer response to SST variations associated with tropical instability waves over the eastern equatorial Pacific. *J. Climate*, **15**, 3379–3393.
- Hastenrath, S., 1991: *Climate Dynamics of the Tropics*. Kluwer Academic, 488 pp.
- Hayes, S. P., M. J. McPhaden, and J. M. Wallace, 1989: The influence of sea surface temperature on surface wind in the eastern equatorial Pacific. *J. Climate*, **2**, 1500–1506.
- Jin, F.-F., J. D. Neelin, and M. Ghil, 1994: El Niño on the devil’s staircase: Annual subharmonic steps to chaos. *Science*, **264**, 70–72.
- Jochum, M., and R. Murtugudde, 2006: Temperature advection by tropical instability waves. *J. Phys. Oceanogr.*, **36**, 592–605.
- Kalnay, E., and Coauthors, 1996: The NCEP/NCAR 40-Year Reanalysis Project. *Bull. Amer. Meteor. Soc.*, **77**, 437–471.
- Kessler, W. S., 2002: Mean three-dimensional circulation in the northeast tropical Pacific. *J. Phys. Oceanogr.*, **32**, 2457–2471.
- , L. M. Rothstein, and D. Chen, 1998: The annual cycle of SST in the eastern tropical Pacific, diagnosed in an ocean GCM. *J. Climate*, **11**, 777–799.
- Kimoto, M., and X. Shen, 1997: Climate variability studies using general circulation models. *The Frontiers of Climate Research II*, S. Sumi, Ed., CCSR/University of Tokyo, 91–116.
- Klein, S. A., and D. L. Hartmann, 1993: The seasonal cycle of low stratiform clouds. *J. Climate*, **6**, 1587–1606.
- Kornfield, J., A. F. Hasler, J. Hanson, and V. E. Suomi, 1967: Photographic cloud climatology from ESSA III and V computer produced mosaics. *Bull. Amer. Meteor. Soc.*, **48**, 878–883.
- Kummerow, C., and Coauthors, 2000: The status of the Tropical Rainfall Measuring Mission (TRMM) after two years in orbit. *J. Appl. Meteor.*, **39**, 1965–1982.
- Langland, R. H., and C.-S. Liou, 1996: Implementation of an E-ε parameterization of vertical subgrid-scale mixing in a regional model. *Mon. Wea. Rev.*, **124**, 905–918.
- Large, W. G., and G. Danabasoglu, 2006: Attribution and impacts of upper-ocean biases in CCSM3. *J. Climate*, **19**, 2325–2346.
- Legeckis, R., 1977: Long waves in the eastern equatorial Pacific: A view of a geostationary satellite. *Science*, **197**, 1177–1181.
- Levitus, S., 1982: *Climatological Atlas of the World Ocean*. NOAA Prof. Paper 13, 173 pp. and 17 microfiche.
- Li, T., and T. F. Hogan, 1999: The role of the annual-mean climate on seasonal and interannual variability of the tropical Pacific in a coupled GCM. *J. Climate*, **12**, 780–792.
- Lietzke, C. E., C. Deser, and T. H. Vonder Haar, 2001: Evolutionary structure of the eastern Pacific double ITCZ based on satellite moisture profile retrievals. *J. Climate*, **14**, 743–751.
- Lin, J. L., and Coauthors, 2006: Tropical intraseasonal variability

- in 14 IPCC AR4 climate models. Part I: Convective signals. *J. Climate*, **19**, 2665–2690.
- Liu, W. T., X. Xie, P. S. Polito, S.-P. Xie, and H. Hashizume, 2000: Atmospheric manifestation of tropical instability waves observed by QuikSCAT and Tropical Rain Measuring Mission. *Geophys. Res. Lett.*, **27**, 2545–2548.
- Luo, J.-J., S. Masson, S. Behera, S. Shingu, and T. Yamagata, 2005: Seasonal climate predictability in a coupled OAGCM using a different approach for ensemble forecasts. *J. Climate*, **18**, 4474–4497.
- Ma, C.-C., C. R. Mechoso, A. W. Robertson, and A. Arakawa, 1996: Peruvian stratus clouds and the tropical Pacific circulation: A coupled ocean–atmosphere GCM study. *J. Climate*, **9**, 1635–1645.
- McCreary, J. P., P. Lu, and Z. Yu, 2002: Dynamics of the Pacific subsurface countercurrents. *J. Phys. Oceanogr.*, **32**, 2379–2404.
- Mechoso, C. R., and Coauthors, 1995: The seasonal cycle over the tropical Pacific in coupled ocean–atmosphere general circulation models. *Mon. Wea. Rev.*, **123**, 2825–2838.
- Miles, N. L., J. Verlinde, and E. E. Clothiaux, 2000: Cloud droplet size distribution in low-level stratiform clouds. *J. Atmos. Sci.*, **57**, 295–311.
- Mitchell, T. P., and J. M. Wallace, 1992: The annual cycle in equatorial convection and sea surface temperature. *J. Climate*, **5**, 1140–1156.
- Neelin, J. D., D. S. Battisti, A. C. Hirst, F. F. Jin, Y. Wakata, T. Yamagata, and S. Zebiak, 1998: ENSO theory. *J. Geophys. Res.*, **103**, 14 261–14 290.
- Nigam, S., and Y. Chao, 1996: Evolution dynamics of tropical ocean–atmosphere annual cycle variability. *J. Climate*, **9**, 3187–3205.
- Nordeng, T. E., 1995: Extended versions of the convective parameterization scheme at ECMWF and their impact on the mean and transient activity of the model in the Tropics. ECMWF Research Department Tech. Memo. 206, 41 pp.
- Norris, J. R., 1998: Low cloud type over the ocean from surface observations. Part II: Geographical and seasonal variations. *J. Climate*, **11**, 383–403.
- Ohfuchi, W., and Coauthors, 2004: 10-km mesh meso-scale resolving simulations of the global atmosphere on the Earth Simulator: Preliminary outcomes of AFES (AGCM for the Earth Simulator). *J. Earth Simul.*, **1**, 8–34.
- Okajima, H., S.-P. Xie, and A. Numaguti, 2003: Interhemispheric coherence of tropical climate variability: Effect of climatological ITCZ. *J. Meteor. Soc. Japan*, **81**, 1371–1386.
- Pacanowski, R. C., 1996: Documentation user's guide and reference manual of MOM2, version 2. GFDL Ocean Tech. Rep. 3.2, 329 pp.
- , and S. G. H. Philander, 1981: Parameterization of vertical mixing in numerical models of tropical oceans. *J. Phys. Oceanogr.*, **11**, 1443–1451.
- Philander, S. C. H., D. Gu, D. Halpern, G. Lambert, N.-C. Lau, T. Li, and R. C. Pacanowski, 1996: The role of low-level stratus clouds in keeping the ITCZ mostly north of the equator. *J. Climate*, **9**, 2958–2972.
- Raymond, D. J., S. K. Esbensen, M. Gregg, and C. S. Bretherton, 2004: EPIC2001 and the coupled ocean–atmosphere system of the tropical east Pacific. *Bull. Amer. Meteor. Soc.*, **85**, 1341–1354.
- Reed, R. K., 1977: On estimating insolation over the ocean. *J. Phys. Oceanogr.*, **7**, 482–485.
- Reynolds, R. W., N. A. Rayner, T. M. Smith, D. C. Stokes, and W. Wang, 2002: An improved in situ and satellite SST analysis for climate. *J. Climate*, **15**, 1609–1625.
- Richter, I., and C. R. Mechoso, 2006: Orographic influences on subtropical stratocumulus. *J. Atmos. Sci.*, **63**, 2585–2601.
- Saji, N. H., S.-P. Xie, and T. Yamagata, 2006: Tropical Indian Ocean variability in the IPCC 20th-century climate simulations. *J. Climate*, **19**, 4397–4417.
- Sakamoto, T., A. Sumi, S. Emori, T. Nishimura, H. Hasumi, T. Suzuki, and M. Kimoto, 2004: Far-reaching effects of the Hawaiian Islands in the CCSR/NIES/FRCGC high-resolution climate model. *Geophys. Res. Lett.*, **31**, L17212, doi:10.1029/2004GL020907.
- Seo, H., A. J. Miller, and J. O. Roads, 2007: The Scripps Coupled Ocean–Atmosphere Regional (SCOAR) model, with applications in the eastern Pacific sector. *J. Climate*, **20**, 381–402.
- Shen, B.-W., R. Atlas, J. D. Chern, O. Reale, S.-J. Lin, T. Lee, and J. Chang, 2006: The 0.125 degree finite-volume general circulation model on the NASA Columbia supercomputer: Preliminary simulations of mesoscale vortices. *Geophys. Res. Lett.*, **33**, L05801, doi:10.1029/2005GL024594.
- Small, R. J., S.-P. Xie, and Y. Wang, 2003: Numerical simulation of atmospheric response to Pacific tropical instability waves. *J. Climate*, **16**, 3723–3741.
- , —, —, S. K. Esbensen, and D. Vickers, 2005: Numerical simulation of boundary layer structure and cross-equatorial flow in the eastern Pacific. *J. Atmos. Sci.*, **62**, 1812–1829.
- Sun, D.-Z., and Z. Liu, 1996: Dynamic ocean–atmosphere coupling: A thermostat for the tropics. *Science*, **272**, 1148–1150.
- Sun, Z., and L. Rikus, 1999: Improved application of exponential sum fitting transmissions to inhomogeneous atmosphere. *J. Geophys. Res.*, **104**, 6291–6303.
- Tiedtke, M., 1989: A comprehensive mass flux scheme for cumulus parameterization in large-scale models. *Mon. Wea. Rev.*, **117**, 1779–1800.
- Timmermann, A., and Coauthors, 2007: The influence of a weakening of the Atlantic meridional overturning circulation on ENSO. *J. Climate*, in press.
- Tripoli, G. J., and W. R. Cotton, 1980: A numerical investigation of several factors contributing to the observed variable intensity of deep convection over south Florida. *J. Appl. Meteor.*, **19**, 1037–1063.
- Wallace, J. M., T. P. Mitchell, and C. Deser, 1989: The influence of sea surface temperature on surface wind in the eastern equatorial Pacific: Seasonal and interannual variability. *J. Climate*, **2**, 1492–1499.
- , E. M. Rusmusson, T. P. Mitchell, V. E. Kousky, E. S. Sarachik, and H. von Storch, 1998: On the structure and evolution of ENSO-related climate variability in the tropical Pacific: Lessons from TOGA. *J. Geophys. Res.*, **103**, 14 214–14 260.
- Wang, C., and J. Picaut, 2004: Understanding ENSO physics—A review. *Earth Climate: The Ocean–Atmosphere Interaction. Geophys. Monogr.*, Vol. 147, Amer. Geophys. Union, 21–69.
- Wang, W., S. Saha, H.-L. Pan, S. Nadiga, and G. White, 2005: Simulation of ENSO in the new NCEP coupled forecast system model (CFS03). *Mon. Wea. Rev.*, **133**, 1574–1593.
- Wang, Y., 2001: An explicit simulation of tropical cyclones with a triply nested movable mesh primitive equation model: TCM3. Part I: Model description and control experiment. *Mon. Wea. Rev.*, **129**, 1370–1394.
- , S.-P. Xie, H. Xu, and B. Wang, 2004a: Regional model simulations of marine boundary layer clouds over the south-

- east Pacific off South America. Part I: Control experiment. *Mon. Wea. Rev.*, **132**, 274–296.
- , H. Xu, and S.-P. Xie, 2004b: Regional model simulations of marine boundary layer clouds over the southeast Pacific off South America. Part II: Sensitivity experiments. *Mon. Wea. Rev.*, **132**, 2650–2668.
- , S.-P. Xie, B. Wang, and H. Xu, 2005: Large-scale atmospheric forcing by southeast Pacific boundary layer clouds: A regional model study. *J. Climate*, **18**, 934–951.
- Wentz, F. J., C. Gentemann, D. Smith, and D. Chelton, 2000: Satellite measurements of sea surface temperature through clouds. *Science*, **288**, 847–850.
- Wittenberg, A. T., A. Rosati, N.-C. Lau, and J. J. Ploshay, 2006: GFDL's CM2 global coupled climate models. Part III: Tropical Pacific climate and ENSO. *J. Climate*, **19**, 698–722.
- Woodruff, S. D., R. J. Slutz, R. L. Jenne, and P. M. Steurer, 1987: A comprehensive ocean–atmosphere dataset. *Bull. Amer. Meteor. Soc.*, **68**, 521–527.
- Wu, L., F. He, and Z. Liu, 2005: Coupled ocean–atmosphere response to north tropical Atlantic SST: Tropical Atlantic dipole and ENSO. *Geophys. Res. Lett.*, **32**, L21712, doi:10.1029/2005GL024222.
- Xie, S.-P., 1994: On the genesis of the equatorial annual cycle. *J. Climate*, **7**, 2008–2013.
- , 1996: Westward propagation of latitudinal asymmetry in a coupled ocean–atmosphere model. *J. Atmos. Sci.*, **53**, 3236–3250.
- , 2004: The shape of continents, air–sea interaction, and the rising branch of the Hadley circulation. *The Hadley Circulation: Past, Present and Future*, H. F. Diaz and R. S. Bradley, Eds., Kluwer Academic, 121–152.
- , and S. G. H. Philander, 1994: A coupled ocean–atmosphere model of relevance to the ITCZ in the eastern Pacific. *Tellus*, **46A**, 340–350.
- , and K. Saito, 2001: Formation and variability of a northerly ITCZ in a hybrid coupled AGCM: Continental forcing and ocean–atmospheric feedback. *J. Climate*, **14**, 1262–1276.
- , M. Ishiwatari, H. Hashizume, and K. Takeuchi, 1998: Coupled ocean–atmospheric waves on the equatorial front. *Geophys. Res. Lett.*, **25**, 3863–3866.
- , H. Xu, W. S. Kessler, and M. Nonaka, 2005: Air–sea interaction over the eastern Pacific warm pool: Gap winds, thermocline dome, and atmospheric convection. *J. Climate*, **18**, 5–25.
- Xu, H., Y. Wang, and S.-P. Xie, 2004: Effects of the Andes on eastern Pacific climate: A regional atmospheric model study. *J. Climate*, **17**, 589–602.
- , S.-P. Xie, Y. Wang, and R. J. Small, 2005: Effects of Central American mountains on the eastern Pacific winter ITCZ and moisture transport. *J. Climate*, **18**, 3856–3873.
- Xu, K.-M., and D. A. Randall, 1996: A semiempirical cloudiness parameterization for use in climate models. *J. Atmos. Sci.*, **53**, 3084–3102.
- Yu, J.-Y., and C. R. Mechoso, 1999: Links between annual variations of Peruvian stratocumulus clouds and of SST in the eastern equatorial Pacific. *J. Climate*, **12**, 3305–3318.
- Yuter, S. E., Y. Serra, and R. A. Houze Jr., 2000: The 1997 Pan American Climate Studies Tropical Eastern Pacific Process Study. Part II: Stratocumulus region. *Bull. Amer. Meteor. Soc.*, **81**, 483–490.
- Zhang, C., 2001: Double ITCZs. *J. Geophys. Res.*, **106**, 11 785–11 792.
- Zhang, R., and T. L. Delworth, 2005: Simulated tropical response to a substantial weakening of the Atlantic thermohaline circulation. *J. Climate*, **18**, 1853–1860.
- Zhang, Y., W. B. Rossow, A. A. Lacis, V. Oinas, and M. I. Mishchenko, 2004: Calculation of radiative fluxes from the surface to top of atmosphere based on ISCCP and other global data sets: Refinements of the radiative transfer model and the input data. *J. Geophys. Res.*, **109**, D19105, doi:10.1029/2003JD004457.